Letter

Realizing robust edge-to-edge transport of atomic momentum states in a dynamically modulated synthetic lattice

Tao Yuan,[1,2] Chao Zeng,[1,2] Yi-Yi Mao,[1,2] Fei-Fei Wu,[1,2] Yan-Jun Xie,[1,2] Wen-Zhuo Zhang,[2] Han-Ning Dai,[1,2,3] Yu-Ao Chen,[1,2,3] and Jian-Wei Pan[1,2,3]

[1]*Hefei National Research Center for Physical Sciences at the Microscale and School of Physical Sciences, University of Science and Technology of China, Hefei 230026, China*

[2]*Shanghai Research Center for Quantum Science and CAS Center for Excellence in Quantum Information and Quantum Physics, University of Science and Technology of China, Shanghai 201315, China*

[3]*Hefei National Laboratory, University of Science and Technology of China, Hefei 230088, China*

(Received 31 January 2023; accepted 16 June 2023; published 12 July 2023)

Quantum transport between distant nodes that is robust to experimental imperfections is essential for quantum information processing. Here we experimentally demonstrate efficient and robust edge-to-edge transport of atomic momentum states in a synthetic lattice of Bose-Einstein condensate, simulating a dynamically modulated Su-Schrieffer-Heeger (SSH) model. This transport process relies on continuously controlling the effective nearest-neighbor couplings in the synthetic lattice, which constructs a unique chain between the left- and right-edge states. The robustness of such transport is protected by the chiral symmetry of the system, demonstrated by subjecting the lattices to coupling-strength disorders. Furthermore, we implement a splitter operation through an SSH model with a topological interface at its center. Our approach provides an efficient single operation to achieve robust momenta transport with potential applications in coherent quantum control in atom optics.

DOI: 10.1103/PhysRevResearch.5.L032005

Introduction. Manipulating and transporting momentum states in atom optics has been widely used in quantum sensing [1,2] and quantum information science [3], such as light-pulse atom interferometry [4], band structure spectroscopy [5], and momentum-lattice-based quantum simulations [6]. Atom interferometers usually rely on highly efficient atom optics to connect the two momentum states, e.g., strong light pulses with the stimulated Raman transitions [7] and quasi-Bragg diffractions [8,9], which allow for the application of many sequential light pulses, enabling momentum transfer and increased sensitivity [10,11]; while simultaneously connecting lots of momentum states with multiple weak Bragg lasers forms synthetic discrete lattices, so-called momentum lattices [12], providing a controllable platform for quantum simulation tasks. Significant progress along this direction also has been achieved in recent years, including realizing different lattice geometries [13], simulating artificial gauge fields [14], and probing topological phase transitions [15]. However, efficient and coherent momenta transfer between distant momentum sites without direct coupling, e.g., edge-to-edge transfer, which is essential for simulating dynamical quantum phenomena in coupled atomic momentum lattices, remains a challenge in experiments.

To achieve such a goal, the most intuitive protocol is to apply a sequence of swap operations between adjacent lattice sites [16], similar to the sequential pulses in atom interferometers. At the same time, the rest of the system remains disconnected. Hence, the initial state is moved toward the target state step by step. Another approach employs suitable preengineered couplings between lattice sites, which is usually rendered the perfect state transfer protocol [17]. As the system evolves, the initial state is coherently transferred to the target state via Rabi-like oscillation schemes [18–20]. Both of these schemes depend strongly on the fine-tuned couplings and the accurate timing of the dynamics. Recent protocols exploit optimal control methods over the driven optical lattice [21] and counterdiabatic control technique in synthetic lattices [22], observing transport dynamics in a few momentum modes. These transport protocols, limited by the inevitable existence of environmental noise and parameter imperfections, are thus not robust.

More recently, inspired by developments in topological pumping [23,24], coherent and robust transport schemes in topological systems have gained much interest [25,26]. Specifically, in a one-dimensional Su-Schrieffer-Heeger (SSH) lattice, the robustness of edge states allows us to transport by adiabatically pumping the edge state from one side to the other [27–30]. Unlike Thouless pumping [31–33], which is quantized bulk state pumping, edge-to-edge transport is controlled only by the coupling strengths and implemented in a complete pump cycle. A few applications of such edge-to-edge topological transport of excitations and energies have been performed in superconducting circuits [34], photonic waveguides [35], and coupled harmonic oscillators [36–38]. However, there are only a few direct experimental demonstrations [38] of the robustness of the protocol. To date, a

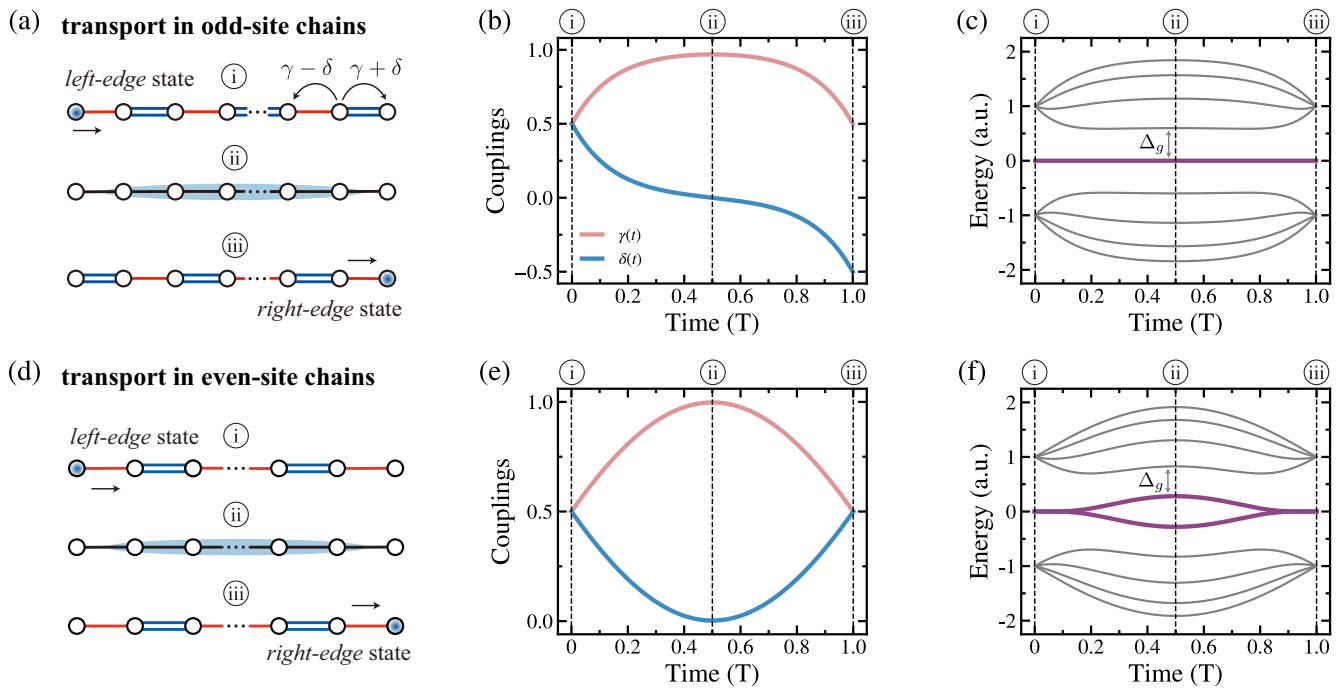

FIG. 1. Protocols of dynamical edge-to-edge transport in SSH chains. (a) Schematics for edge-to-edge transport in a one-dimensional (1D) odd-site SSH chain. The dynamical modulation of coupling strengths induces the transport of a left-edge state into a right-edge state. (b), (c) The modulations of the coupling strengths (red and blue lines) for an SSH chain with $L=9$ and the instantaneous energy spectrum of the system. The thick gray line corresponds to the zero-energy topological edge mode. (d) Schematics for edge-to-edge transport in a 1D even-site SSH chain. (e), (f) The modulations of the coupling strengths (red and blue lines) for an SSH chain with $L=10$ and the instantaneous energy spectrum of the system. The thick gray lines correspond to the two topological edge modes. Δ_g represents the minimal energy gap between the edge modes and the bulk states during the transport process.

time-controlled topological pump of momentum states remains elusive, and as a result, on-demand robust transport of momenta in a connected atomic momentum lattice has yet to be achieved.

Here, we report on the realization of efficient and robust edge-to-edge transport of atomic momentum states in a synthetic lattice of Bose-Einstein condensed (BEC) states via a scheme of topological pumping. This scheme applies a time-dependent sequence to the staggered nearest-neighbor (NN) couplings along the lattice, modulated through the stimulated Bragg transitions. We implement two distinct transport protocols with optimized sequences for both odd- and even-site chains, achieving effective transport for more than ten momentum sites. Furthermore, the robustness of the topological transport scheme is confirmed by comparing it with another perfect state transfer scheme when subjected to coupling strength disorders. Moreover, we extend the application of this dynamical transport for coherent splitter operation. With a topological interface in the SSH chain, the initial state at the central site is first transported into the two-end sites with equal probabilities and later recombined at the central site again, indicating the coherent operation of the splitter operation. Our experiments enrich the study of dynamical phenomena in momentum lattices and will provide inspiration for the spatial transport and distribution of entanglement in disorder systems.

The transport protocol. We consider the Su-Schrieffer-Heeger model as the transport channel, which is a linear quantum chain of macroscopically separated sites, as shown in Fig. 1. The Hamiltonian of the system is given by [39]

$$\hat{H}(t) = -\sum_{n=0}^{L-2} [\gamma(t) - (-1)^n \delta(t)][\hat{a}_{n+1}^\dagger \hat{a}_n + \text{H.c.}], \qquad (1)$$

where $\hat{a}_n$ and $\hat{a}_n^\dagger$ are the annihilation and creation operators acting on the lattice site of n, respectively. L denotes the length of the SSH chain. $\gamma(t) \pm \delta(t)$ are the time-dependent NN couplings of even and odd bonds in the lattice. In the thermodynamic limit, the SSH model is known to exhibit two topologically distinct phases, topologically nontrivial for $\delta(t) > 0$ and topologically trivial for $\delta(t) < 0$, separated by a topological phase transition point at $\delta(t) = 0$. The distinct topological character of the two phases is reflected in the difference in their bulk topological invariant, i.e., the winding number, for which $+1$ in the topologically nontrivial phase and 0 in the topologically trivial phase [40].

Due to the bulk-edge correspondence, when SSH chains are in a topological phase, there are additional disorder-resilient edge modes bound to the open ends of the chain [41]. We first consider the odd-sized SSH chains, as shown in Fig. 1(a). Due to the chiral symmetry, a zero-energy edge state always exists in the odd-sized SSH chain, which is protected against the disorder that preserves the chiral symmetry of the system [28]. When $\delta(t) > 0$ or $\delta(t) < 0$, the edge state is localized at the left or right side of the chain. One can first set $\gamma(0) = \delta(0) = \gamma_0/2$ and the leftmost edge site is decoupled

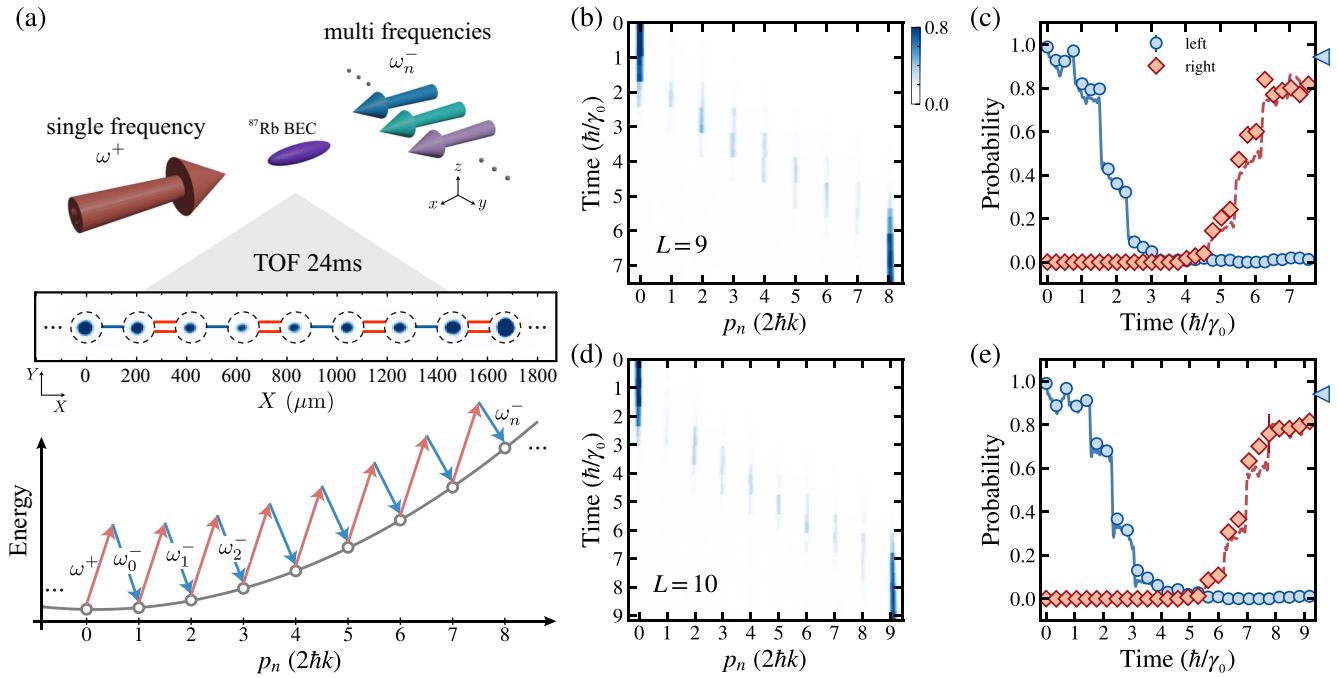

FIG. 2. Demonstration of edge-to-edge transport in a momentum lattice. (a) Top: Illustration of the experimental setup of the momentum lattice. The BEC is illuminated by a pair of counterpropagating Bragg beams, one of which (left-going laser) contains multiple discrete frequency components (ω_n^-). These two beams resonantly couple a set of momentum states, forming a synthetic lattice. By tuning staggered couplings in even and odd bonds of the lattice, we effectively simulate a tight-binding SSH model. Middle: A typical experimental absorption image of the atom cloud for different momentum states after a time of flight of 24 ms. Bottom: The dispersion relation and depiction of Bragg transition pathways for the nearest-neighbor couplings. (b), (d) The experimentally observed dynamics of site occupations during the transport in the SSH chains of length $L=9$ and $L=10$, respectively. (c), (e) The evolution of occupations for the left- (blue) and right-edge (red) sites during the transport in the SSH chains of length $L=9$ and $L=10$, respectively. The circles and diamonds correspond to the experimental data, and the lines correspond to the numerical simulations. The triangular markers on the side indicate the calculated probability using ideal effective Hamiltonian. The error bars represent the 1σ standard deviation of the measurements.

from the rest of the chain, which can be used for the input excitation. Afterwards, as shown in Fig. 1(b), adiabatic modulations of the coupling strengths with $\gamma_o(t) = \gamma_0 F_o(\alpha, t, T)$ and $\delta_o(t) = \gamma_0 K_o(\alpha, t, T)$ are applied to the system, where γ_0 is the typical coupling strength, T is the total transport time, and α is the tuning parameter (see the Supplemental Material for details [42]). The edge mode is at zero energy and well separated from the bulk states, as shown in Fig. 1(c). Such a modulation will drive the input state across the chain, producing a right-localized edge state, thus implementing dynamical edge-to-edge transport.

Similarly, for even-sized SSH chains in the nontrivial topological phase $\delta(t) > 0$, two zero-energy edge modes appear at the two ends of the chain, as shown in Fig. 1(d). We send the input excitation to the leftmost edge site and set $\gamma(0) = \delta(0) = \gamma_0/2$. Then, we modulate the SSH chain by another dynamical sequence with $\gamma_e(t) = \gamma_0 F_e(\alpha, t, T)$ and $\delta_e(t) = \gamma_0 K_e(\alpha, t, T)$ [see Figs. 1(e) and 1(f)]. During the modulation, the two edge states become hybridized, and the input state is transported to the right edge.

The transport efficiency, i.e., the occupation probability at the target state, is used to characterize the performance of the transport process, $\mathcal{I}_R = |\langle L-1|\ \Psi(t=T)\rangle|^2$, where $\{|n = 0, 1, \ldots, L-1\rangle\}$ represents the Hilbert space of the model, $|\Psi(t)\rangle = \sum_{n=0}^{L-1} c_n(t)|n\rangle$ denotes the wave function of the system during the transport process, and c_n are the complex amplitudes. By carefully choosing the modulation parameters of (α, T) to maximize the transport efficiency, we derive optimized edge-to-edge transport sequences for different transport distances [42]. The broad optimal parameter regions of (α, T) for transport efficiency higher than 0.9 indicates the flexibility of performing efficient edge-to-edge transport. In the experiments, we can choose transport sequences with short time costs to perform fast transport. At the same time, we can choose longer transport times for higher adiabaticity to perform the robustness of the transport process.

Experimental setup. The experiment starts with a weakly trapped ^{87}Rb BEC of $\sim 10^5$ atoms, with residual harmonic confinement of trapping frequencies $\sim 2\pi \times (15, 60, 40)$ Hz, as depicted in Fig. 2(a). We then apply a pair of counterpropagating lasers (wavelength $\lambda = 1064$ nm) to drive Bragg transitions that can change the atomic momentum in increments of $2\hbar k$ (with $k = 2\pi/\lambda$ and $\hbar$ being the reduced Planck's constant). While one of the beams has a single frequency component (ω^+), the other beam is engineered to have multiple discrete frequency components (ω_n^-), which is realized by using a pair of acousto-optic modulators to write a controlled spectrum of frequency components onto the lattice beam. Together, these two beams drive a set of two-photon Bragg transitions, forming a synthetic lattice in momentum

space [12,42]. The lattice sites are defined on discrete momentum states of $p_n = 2n\hbar k$ and energies $E_n = 2n^2\hbar^2k^2/m$, where n is the site index and m is the atomic mass. Here we treat the dispersion relation of BEC as that of free particles, with weak interactions [43,44] and loose trapping potential [45], making this a good approximation. By controlling the strengths and phases of the Bragg laser fields, we can dynamically modulate each link in the lattice to perform edge-to-edge transport. In our experiments, we set the typical coupling strength to $\gamma_0 = 2\pi\hbar \times 2.00(1)$ kHz, corresponding to the equivalent units of the coupling time $\hbar/\gamma_0 \approx 80$ μs.

Following the transport sequence, all the laser beams are extinguished, and the atoms are allowed to freely fall and expand in time of flight (TOF), which will map the different momentum states into real space. After a TOF time of 24 ms, we take an image of the density distribution of the atomic cloud and derive the populations for each momentum lattice site, as shown in Fig. 2(a). Thus, the whole dynamic evolution during dynamic transport is obtained by monitoring the atomic populations at different transport times.

Demonstration of edge-to-edge transport. We first demonstrate dynamical edge-to-edge transport in odd-sized SSH chains. For example, in an SSH chain comprising nine sites $L = 9$, we choose the transport time of $T = 7.54\hbar/\gamma_0$ and the optimized tuning parameter at $\alpha = 6.87$, as shown in Fig. 1(b). Under such a setting, the minimal energy gap during transport is $\Delta_g = 0.60\gamma_0$ and the transport time is larger than the characteristic timescale of $\Delta_g^{-1} = 1.66\hbar/\gamma_0$, meeting the adiabatic condition [46]. As shown in Fig. 2(b), all atoms are initially prepared at the left-edge site for the zero momentum state $|n = 0\rangle$. Then, the atoms are gradually transported to the right side of the chain, following the dynamic edge-to-edge transport modulation. In the end, the population of atoms is successfully transported to the right-edge site $|n = 8\rangle$, with an efficiency $\mathcal{I}_R = 0.82(2)$, as shown in Fig. 2(c).

Next, we implement the dynamical edge-to-edge transport in an even-sized SSH chain at $L = 10$, with a transport time of $T = 9.17\hbar/\gamma_0$ and the optimized tuning parameter at $\alpha = 0.15$ [see Fig. 1(e)]. This sequence fulfills the adiabatic condition, which requires the minimal transport time of $\Delta_g^{-1} = 1.83\hbar/\gamma_0$. Meanwhile, the global adiabaticity of the hybridization of the two edge modes ($|\Psi_L\rangle$ and $|\Psi_R\rangle$) can be expressed by the area theorem [47], which requires $\int_0^T \langle\Psi_L|\hat{H}(t)|\Psi_R\rangle dt > \pi/2$. With our setting parameters for $L = 10$, the area is approximately 0.6π. Thus, the atoms are effectively transported from $|n = 0\rangle$ to $|n = 9\rangle$ with an efficiency of $\mathcal{I}_R = 0.81(2)$, as shown in Figs. 2(d) and 2(e).

Thus, we can transfer to any lattice site in the chain on demand. For longer chains of $L \leqslant 14$, the achieved efficiencies are higher than 0.5. Numerical simulations with the time-evolved Gross-Pitaevskii equations (GPEs) also agree well with our experiments [42]. One limiting factor of transport efficiency is the effect of the trapping potential. By loosening the trapping potential along the direction of imparted momentum, higher transport efficiency could be achieved in the loose trapping potential [42].

Robustness to coupling strength disorders. One of the advantages of such topological transport is the robustness against imperfections of the system. Here, we focus on the robustness of the coupling-strength disorders in topological transport, which respect the chiral symmetry of SSH chains [40]. One can easily implement the coupling-strength disorders by controlling the Bragg transition strengths between discrete momentum states. In particular, we take the odd chains as an example and set each of the coupling terms to $\gamma_n(t) = \gamma_o(t)(1+W\xi_n)$ and $\delta_n(t) = \delta_o(t)(1+W\zeta_n)$, where ξ_n and ζ_n are independent random real numbers chosen uniformly from the range $[-1, 1]$, and W is the dimensionless strength of disorder.

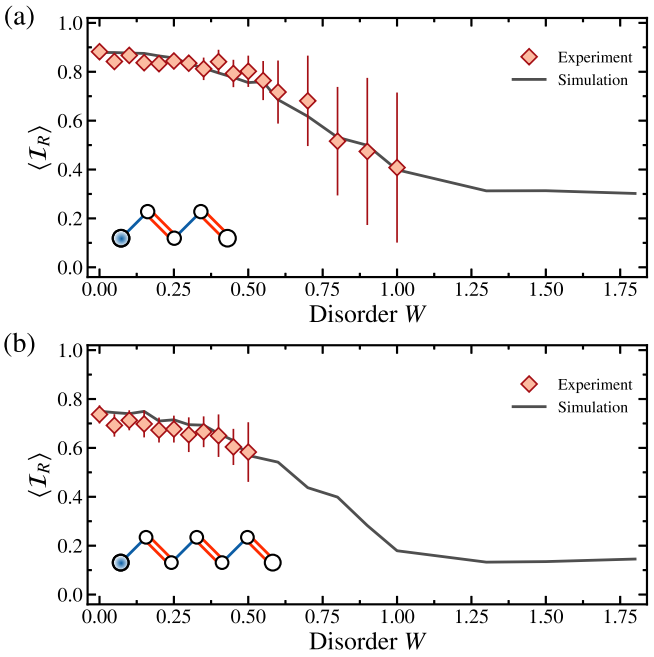

FIG. 3. Robustness against coupling strength disorders. (a), (b) The mean transport efficiencies for adiabatic edge-to-edge transport are measured in disordered SSH chains of $L = 5$ and $L = 7$, respectively. The red diamond points are experimental data averaged over 20 independent disorder configurations. The error bars represent one standard deviation. The gray lines represent the numerical simulations with experimental parameters for 100 independent disorder configurations.

The performance of the transfer process in disordered systems can be characterized by the mean transport efficiency $\langle\mathcal{I}_R\rangle$. For example, in a clean chain with five sites $L = 5$, the designed parameters for the transport process are $\alpha = 1.49$ and $T = 25\hbar/\gamma_0$. The transport efficiency in a clean system is approximately 0.88, as shown in Fig. 3(a). With the increase in the disorder strength, the transport remains efficient, where the efficiency can still achieve $\langle\mathcal{I}_R\rangle = 0.80$ at $W = 0.5$. Similar robust transport performance is measured for a chain with $L = 7$ at $\alpha = 1.89$ and $T = 25\hbar/\gamma_0$, as shown in Fig. 3(b). Here, we have taken fewer experimental data at larger W when the efficiency is below 0.5. Since our experimental results agree well with the GPE simulations, we have taken more data through numerical simulation.

To analyze the robustness of the transport process, we define the critical disorder strength W_c, corresponding to an efficiency of half the maximum value. From the GPE simulations, the critical disorder strengths are about 0.90 and

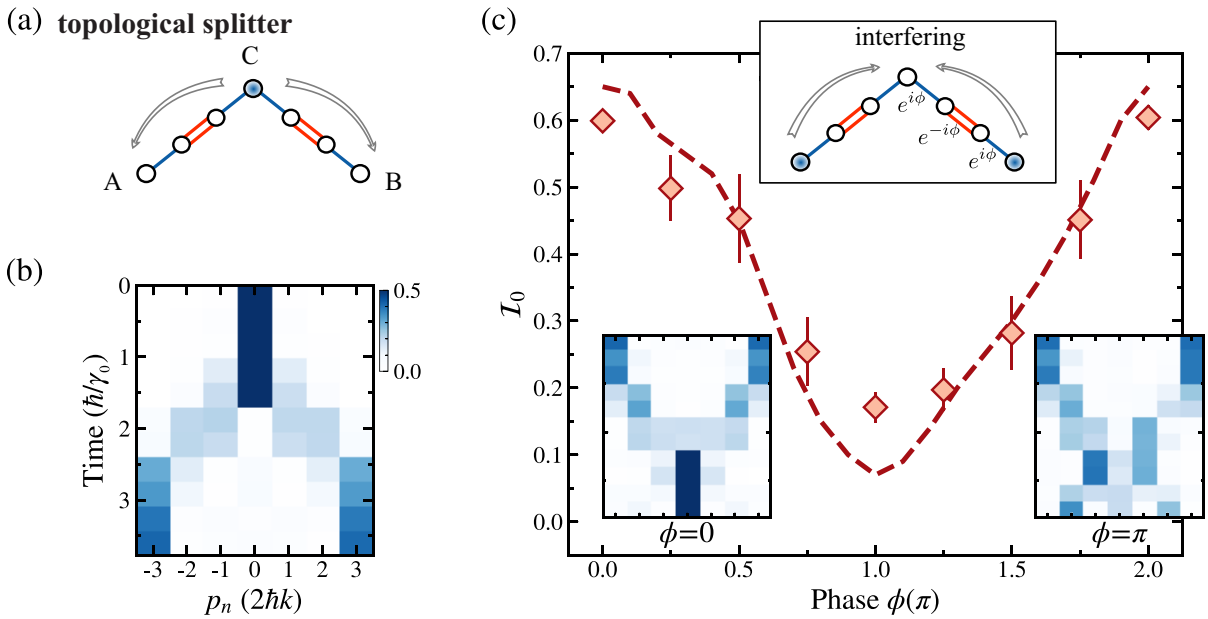

FIG. 4. Implementing a splitter operation. (a) Schematic of a modified SSH chain with an interface site introduced at the center. (b) Dynamics of site populations during the splitter operation. The initial state at the center site are split and transported to the two-end sites with equal probabilities. (c) The interfering process from the two-end sites to the center with controlled phases ϕ on the right side of the chain. The red diamonds represent experimental data, and the dashed line is the numerical simulation by GPE. Inset on top: Schematic of the interfering process. Inset on bottom: Dynamics of the interfering process at $\phi=0$ and $\phi=\pi$, respectively.

0.80 for our transport protocol at $L=5$ and 7, respectively. Moreover, it is found that a wide energy gap in the SSH chain favors the topological chain to realize robust transport. When further increasing the disorder strength, the transport efficiency reduces significantly due to decreasing the energy gap, indicating the breakdown of the adiabaticity [35,42,47]. For comparison, we send the same increasing disorder to a nontopological protocol, i.e., the perfect state transfer method, where the mean transport efficiency drops much faster than the topological method [42].

Implementing a splitter operation. Furthermore, we extend the application of the dynamical edge-to-edge transport protocol to implement a coherent splitter operation [48,49], which has been recently designed for engineering two-way and three-way splitting based upon different lattice structures [50,51] for applications in matter wave operations and atom optics. The simplest splitter operation, in which the initial state prepared at the central site can be later observed at the two-end sites with equal probabilities and recombined at the central site again, can now be first realized in ultracold atoms based on the dynamical edge-to-edge transport in momentum lattices.

Utilizing the feasibility of site-resolved modulation of the momentum lattice, we construct a unique transport channel in an SSH chain with seven lattice sites, where an interface site at the center connects both of its nearest-neighbor sites with weak couplings, as shown in Fig. 4(a). Then, we perform dynamic edge-to-edge transport following the modulations with $\alpha=0.3$ and $T=3.77\hbar/\gamma_0$. At the end of the transport, the input state initially in the central site p_0 is transported to the two end sites $p_{\pm3}$, with a balanced population $\mathcal{I}_{-3}=0.41(1)$ and $\mathcal{I}_3=0.41(0)$, as shown in Fig. 4(b).

Afterward, the split state is reflected by the two ends and sent back to the center by the same transport process for interference. As shown in Fig. 4(c), we introduce additional modulated phases ϕ for couplings at the right part of the chain. Finally, the atomic occupations at different sites are measured for the modulated phase from $\phi=0$ to $\phi=2\pi$. We use the central site occupancy $\mathcal{I}_0$ to characterize the interference. When the phase is $\phi=0$, the states at two end sites are transported to the central site again, which interferes and gives out a peak occupancy $\mathcal{I}_0=0.60(2)$, while the site population at the central site gives out a minimal value $\mathcal{I}_0=0.17(2)$ when the phase is $\phi=\pi$. Thus, the occupation probabilities $\mathcal{I}_0$ at different modulated phases show a typical interferometric pattern, showing the phase coherence of the splitter operation.

Summary. In summary, we have successfully demonstrated dynamic and robust edge-to-edge transport with a single operation in the SSH model based on the momentum lattices of BEC. We also quantitatively identify the robustness of the protocol by adding controlled disorders into the coupling strength, highlighting the topological protection due to the chiral symmetry of the system. A splitter operation is further demonstrated based on the edge-to-edge transport protocol, where a state can be coherently split and recombined, showing the potential application in atom interferometry. The transfer protocol can be further extended by introducing site-energy modulations [47,49] in the Rice-Mele model, which is more advantageous in terms of robustness against coupling disorder and on-site disorder. At the same time, the transfer scheme can also be extended by introducing next-nearest-neighbor couplings [14,52] or non-Hermitian terms [53,54], which will activate the shortcut for nonadiabatic edge-to-edge transport.

By modulating multiple Bragg lasers, our approach can also be implemented for high-order diffractions in the quasi-Bragg regime for atom interferometry [8,9]. Our work could lead to novel applications in matter wave manipulations and reliable quantum state transfer, which could improve coherent quantum control in atom optics and benefit the investigation of topological dynamics.

Acknowledgments. The authors would like to thank Z.-S. Yuan and B. Yan for useful discussions. This work is supported by the National Natural Science Foundation of China (Grant No. 12074367), the Fundamental Research Funds for the Central Universities, Anhui Initiative in Quantum Information Technologies, the Program of Shanghai Academic/Technology Research Leader (Grant No. 18XD1404000), the National Key Research and Development Program of China (Grant No. 2020YFA0309804), Shanghai Municipal Science and Technology Major Project (Grant No. 2019SHZDZX01), the Innovation Program for Quantum Science and Technology (Grant No. 2021ZD0302002), the Chinese Academy of Sciences.

[1] A. D. Cronin, J. Schmiedmayer, and D. E. Pritchard, Optics and interferometry with atoms and molecules, Rev. Mod. Phys. **81**, 1051 (2009).

[2] K. Bongs, M. Holynski, J. Vovrosh, P. Bouyer, G. Condon, E. Rasel, C. Schubert, W. P. Schleich, and A. Roura, Taking atom interferometric quantum sensors from the laboratory to real-world applications, Nat. Rev. Phys. **1**, 731 (2019).

[3] A. Acín, I. Bloch, H. Buhrman, T. Calarco, C. Eichler, J. Eisert, D. Esteve, N. Gisin, S. J. Glaser, F. Jelezko, S. Kuhr, M. Lewenstein, M. F. Riedel, P. O. Schmidt, R. Thew, A. Wallraff, I. Walmsley, and F. K. Wilhelm, The quantum technologies roadmap: a European community view, New J. Phys. **20**, 080201 (2018).

[4] T. Kovachy, P. Asenbaum, C. Overstreet, C. A. Donnelly, S. M. Dickerson, A. Sugarbaker, J. M. Hogan, and M. A. Kasevich, Quantum superposition at the half-metre scale, Nature (London) **528**, 530 (2015).

[5] P. T. Ernst, S. Götze, J. S. Krauser, K. Pyka, D.-S. Lühmann, D. Pfannkuche, and K. Sengstock, Probing superfluids in optical lattices by momentum-resolved Bragg spectroscopy, Nat. Phys. **6**, 56 (2010).

[6] E. J. Meier, F. A. An, A. Dauphin, M. Maffei, P. Massignan, T. L. Hughes, and B. Gadway, Observation of the topological Anderson insulator in disordered atomic wires, Science **362**, 929 (2018).

[7] J. M. McGuirk, M. J. Snadden, and M. A. Kasevich, Large Area Light-Pulse Atom Interferometry, Phys. Rev. Lett. **85**, 4498 (2000).

[8] H. Müller, S.-W. Chiow, Q. Long, S. Herrmann, and S. Chu, Atom Interferometry with up to 24-Photon-Momentum-Transfer Beam Splitters, Phys. Rev. Lett. **100**, 180405 (2008).

[9] S. Chiow, T. Kovachy, H.-C. Chien, and M. A. Kasevich, 102$\hbar$k Large Area Atom Interferometers, Phys. Rev. Lett. **107**, 130403 (2011).

[10] A. Peters, K. Y. Chung, and S. Chu, High-precision gravity measurements using atom interferometry, Metrologia **38**, 25 (2001).

[11] B. Plotkin-Swing, D. Gochnauer, K. E. McAlpine, E. S. Cooper, A. O. Jamison, and S. Gupta, Three-Path Atom Interferometry with Large Momentum Separation, Phys. Rev. Lett. **121**, 133201 (2018).

[12] B. Gadway, Atom-optics approach to studying transport phenomena, Phys. Rev. A **92**, 043606 (2015).

[13] P. Lauria, W.-T. Kuo, N. R. Cooper, and T. Barreiro, Experimental Realization of a Fermionic Spin-Momentum Lattice, Phys. Rev. Lett. **128**, 245301 (2022).

[14] F. A. An, E. J. Meier, and B. Gadway, Engineering a Flux-Dependent Mobility Edge in Disordered Zigzag Chains, Phys. Rev. X **8**, 031045 (2018).

[15] D. Xie, T.-S. Deng, T. Xiao, W. Gou, T. Chen, W. Yi, and B. Yan, Topological Quantum Walks in Momentum Space with a Bose-Einstein Condensate, Phys. Rev. Lett. **124**, 050502 (2020).

[16] O. Romero-Isart and J.-J. García-Ripoll, Quantum ratchets for quantum communication with optical superlattices, Phys. Rev. A **76**, 052304 (2007).

[17] M. Christandl, N. Datta, A. Ekert, and A. J. Landahl, Perfect State Transfer in Quantum Spin Networks, Phys. Rev. Lett. **92**, 187902 (2004).

[18] R. J. Chapman, M. Santandrea, Z. Huang, G. Corrielli, A. Crespi, M.-H. Yung, R. Osellame, and A. Peruzzo, Experimental perfect state transfer of an entangled photonic qubit, Nat. Commun. **7**, 11339 (2016).

[19] X. Li, Y. Ma, J. Han, T. Chen, Y. Xu, W. Cai, H. Wang, Y. P. Song, Z.-Y. Xue, Z.-Q. Yin, and L. Sun, Perfect Quantum State Transfer in a Superconducting Qubit Chain with Parametrically Tunable Couplings, Phys. Rev. Appl. **10**, 054009 (2018).

[20] T. Tian, S. Lin, L. Zhang, P. Yin, P. Huang, C. Duan, L. Jiang, and J. Du, Perfect coherent transfer in an on-chip reconfigurable nanoelectromechanical network, Phys. Rev. B **101**, 174303 (2020).

[21] N. Dupont, G. Chatelain, L. Gabardos, M. Arnal, J. Billy, B. Peaudecerf, D. Sugny, and D. Guéry-Odelin, Quantum state control of a bose-einstein condensate in an optical lattice, PRX Quantum **2**, 040303 (2021).

[22] E. J. Meier, K. Ngan, D. Sels, and B. Gadway, Counterdiabatic control of transport in a synthetic tight-binding lattice, Phys. Rev. Res. **2**, 043201 (2020).

[23] S. Nakajima, T. Tomita, S. Taie, T. Ichinose, H. Ozawa, L. Wang, M. Troyer, and Y. Takahashi, Topological Thouless pumping of ultracold fermions, Nat. Phys. **12**, 296 (2016).

[24] J. Tangpanitanon, V. M. Bastidas, S. Al-Assam, P. Roushan, D. Jaksch, and D. G. Angelakis, Topological Pumping of Photons in Nonlinear Resonator Arrays, Phys. Rev. Lett. **117**, 213603 (2016).

[25] N. Y. Yao, C. R. Laumann, A. V. Gorshkov, H. Weimer, L. Jiang, J. I. Cirac, P. Zoller, and M. D. Lukin, Topologically protected quantum state transfer in a chiral spin liquid, Nat. Commun. **4**, 1585 (2013).

[26] C. Dlaska, B. Vermersch, and P. Zoller, Robust quantum state transfer via topologically protected edge channels in dipolar arrays, Quantum Sci. Technol. **2**, 015001 (2017).

[27] N. Lang and H. P. Büchler, Topological networks for quantum communication between distant qubits, npj Quantum Inf. **3**, 47 (2017).

[28] F. Mei, G. Chen, L. Tian, S.-L. Zhu, and S. Jia, Robust quantum state transfer via topological edge states in superconducting qubit chains, Phys. Rev. A **98**, 012331 (2018).

[29] N. E. Palaiodimopoulos, I. Brouzos, F. K. Diakonos, and G. Theocharis, Fast and robust quantum state transfer via a topological chain, Phys. Rev. A **103**, 052409 (2021).

[30] S. Longhi, Topological pumping of edge states via adiabatic passage, Phys. Rev. B **99**, 155150 (2019).

[31] D. J. Thouless, Quantization of particle transport, Phys. Rev. B **27**, 6083 (1983).

[32] M. Lohse, C. Schweizer, O. Zilberberg, M. Aidelsburger, and I. Bloch, A Thouless quantum pump with ultracold bosonic atoms in an optical superlattice, Nat. Phys. **12**, 350 (2016).

[33] M. Jürgensen, S. Mukherjee, and M. Rechtsman, Quantized nonlinear Thouless pumping, Nature (London) **596**, 63 (2021).

[34] J. Deng, H. Dong, C. Zhang, Y. Wu, J. Yuan, X. Zhu, F. Jin, H. Li, Z. Wang, H. Cai, C. Song, H. Wang, J. Q. You, and D.-W. Wang, Observing the quantum topology of light, Science **378**, 966 (2022).

[35] W. Liu, C. Wu, Y. Jia, S. Jia, G. Chen, and F. Chen, Observation of edge-to-edge topological transport in a photonic lattice, Phys. Rev. A **105**, L061502 (2022).

[36] I. H. Grinberg, M. Lin, C. Harris, W. A. Benalcazar, C. W. Peterson, T. L. Hughes, and G. Bahl, Robust temporal pumping in a magnetomechanical topological insulator, Nat. Commun. **11**, 974 (2020).

[37] W. Cheng, E. Prodan, and C. Prodan, Experimental Demonstration of Dynamic Topological Pumping across Incommensurate Bilayered Acoustic Metamaterials, Phys. Rev. Lett. **125**, 224301 (2020).

[38] T. Tian, Y. Zhang, L. Zhang, L. Wu, S. Lin, J. Zhou, C.-K. Duan, J.-H. Jiang, and J. Du, Experimental Realization of Nonreciprocal Adiabatic Transfer of Phonons in a Dynamically Modulated Nanomechanical Topological Insulator, Phys. Rev. Lett. **129**, 215901 (2022).

[39] W. P. Su, J. R. Schrieffer, and A. J. Heeger, Solitons in Polyacetylene, Phys. Rev. Lett. **42**, 1698 (1979).

[40] J. K. Asbóth, L. Oroszlány, and A. Pályi, *A Short Course on Topological Insulators: Band Structure and Edge States in One and Two Dimensions*, Lecture Notes in Physics Vol. 919 (Springer, New York, 2016).

[41] N. R. Cooper, J. Dalibard, and I. B. Spielman, Topological bands for ultracold atoms, Rev. Mod. Phys. **91**, 015005 (2019).

[42] See Supplemental Material at http://link.aps.org/supplemental/10.1103/PhysRevResearch.5.L032005 for more details on the experimental method, numerical simulations, and further discussion about the robustness of edge-to-edge transport.

[43] R. Ozeri, N. Katz, J. Steinhauer, and N. Davidson, *Colloquium*: Bulk Bogoliubov excitations in a Bose-Einstein condensate, Rev. Mod. Phys. **77**, 187 (2005).

[44] F. A. An, E. J. Meier, J. Ang'ong'a, and B. Gadway, Correlated Dynamics in a Synthetic Lattice of Momentum States, Phys. Rev. Lett. **120**, 040407 (2018).

[45] S. Utsunomiya, L. Tian, G. Roumpos, C. W. Lai, N. Kumada, T. Fujisawa, M. Kuwata-Gonokami, A. Löffler, S. Höfling, A. Forchel, and Y. Yamamoto, Observation of Bogoliubov excitations in exciton-polariton condensates, Nat. Phys. **4**, 700 (2008).

[46] S. Jansen, M.-B. Ruskai, and R. Seiler, Bounds for the adiabatic approximation with applications to quantum computation, J. Math. Phys. **48**, 102111 (2007).

[47] S. Longhi, G. L. Giorgi, and R. Zambrini, Landau-zener topological quantum state transfer, Adv. Quantum Technol. **2**, 1800090 (2019).

[48] L. Qi, G.-L. Wang, S. Liu, S. Zhang, and H.-F. Wang, Engineering the topological state transfer and topological beam splitter in an even-sized Su-Schrieffer-Heeger chain, Phys. Rev. A **102**, 022404 (2020).

[49] L. Qi, Y. Xing, X.-D. Zhao, S. Liu, S. Zhang, S. Hu, and H.-F. Wang, Topological beam splitter via defect-induced edge channel in the Rice-Mele model, Phys. Rev. B **103**, 085129 (2021).

[50] M. Makwana, R. Craster, and S. Guenneau, Topological beam-splitting in photonic crystals, Opt. Express **27**, 16088 (2019).

[51] S. Zheng, J. Zhang, G. Duan, Z. Jiang, X. Man, D. Yu, and B. Xia, Topological network and valley beam splitter in acoustic biaxially strained moiré superlattices, Phys. Rev. B **105**, 184104 (2022).

[52] F. M. D'Angelis, F. A. Pinheiro, D. Guéry-Odelin, S. Longhi, and F. Impens, Fast and robust quantum state transfer in a topological Su-Schrieffer-Heeger chain with next-to-nearest-neighbor interactions, Phys. Rev. Res. **2**, 033475 (2020).

[53] Q. Liang, D. Xie, Z. Dong, H. Li, H. Li, B. Gadway, W. Yi, and B. Yan, Dynamic Signatures of Non-Hermitian Skin Effect and Topology in Ultracold Atoms, Phys. Rev. Lett. **129**, 070401 (2022).

[54] E. Riva, G. Castaldini, and F. Braghin, Adiabatic edge-to-edge transformations in time-modulated elastic lattices and non-Hermitian shortcuts, New J. Phys. **23**, 093008 (2021).